Versatile silicon-waveguide supercontinuum for coherent mid-infrared spectroscopy

Nima Nader,[1,a] Daniel L. Maser,[2,3] Flavio C. Cruz,[2,4] Abijith Kowligy,[2]
Henry Timmers,[2] Jeff Chiles,[1] Connor Fredrick,[2,3] Daron A. Westly,[5]
Sae Woo Nam,[1] Richard P. Mirin,[1] Jeffrey M. Shainline,[1] and Scott Diddams[2,3]

[1]*Applied Physics Division, National Institute of Standards and Technology, 325 Broadway, Boulder, Colorado 80305, USA*

[2]*Time and Frequency Division, National Institute of Standards and Technology, 325 Broadway, Boulder, Colorado 80305, USA*

[3]*Department of Physics, University of Colorado Boulder, 2000 Colorado Boulevard, Boulder, Colorado 80309, USA*

[4]*Instituto de Fisica Gleb Wataghin, Universidade Estadual de Campinas, Campinas, SP 13083-859, Brazil*

[5]*Center for Nanoscale Science and Technology, National Institute of Standards and Technology, 100 Bureau Drive, Gaithersburg, Maryland 20899, USA*

Laser frequency combs, with their unique combination of precisely defined spectral lines and broad bandwidth, are a powerful tool for basic and applied spectroscopy. Here, we report offset-free, mid-infrared frequency combs and dual-comb spectroscopy through supercontinuum generation in silicon-on-sapphire waveguides. We leverage robust fabrication and geometrical dispersion engineering of nanophotonic waveguides for multi-band, coherent frequency combs spanning 70 THz in the mid-infrared (2.5 μm–6.2 μm). Precise waveguide fabrication provides significant spectral broadening with engineered spectra targeted at specific mid-infrared bands. We characterize the relative-intensity-noise of different bands and show that the measured levels do not pose any limitation for spectroscopy applications. Additionally, we use the fabricated photonic devices to demonstrate dual-comb spectroscopy of a carbonyl sulfide gas sample at 5 μm. This work forms the technological basis for applications such as point sensors for fundamental spectroscopy, atmospheric chemistry, trace and hazardous gas detection, and biological microscopy. *© 2018 Author(s). All article content, except where otherwise noted, is licensed under a Creative Commons Attribution (CC BY) license (http://creativecommons.org/licenses/by/4.0/).* https://doi.org/10.1063/1.5006914

I. INTRODUCTION

Spectroscopy has been a primary scientific tool for studying nature, leading to seminal advances in astronomy, quantum physics, chemistry, and biology. The coherent light from a laser provides a powerful spectroscopic tool with the properties of high spectral resolution, wavelength tunability, and a well-defined Gaussian beam enabling high intensity focusing and long-distance propagation. Frequency comb lasers combine the above qualities in addition to a broad spectrum of precisely defined optical lines (the comb) that can be absolutely referenced to radio frequencies (RF) or atomic frequency standards.[1–3] This has led to a variety of new spectroscopic advances.[4–13]

While frequency combs were initially developed for the visible and near-infrared spectral regions, more recent research has focused on extending their coverage to the mid-infrared (mid-IR).[14] This spectral region is of great interest because it is where many molecules including greenhouse gases, poisonous agents, explosives, and organics show distinctive ro-vibrational absorption fingerprints.[14]

---

[a]Electronic mail: nader.nima@gmail.com and nima.nader@nist.gov

The development of a practical, broadband, and low-noise mid-IR frequency comb with moderate power could dramatically improve frequency precision, sensitivity, and data acquisition rates compared to conventional techniques such as Fourier-transform-infrared (FTIR) spectroscopy. Different approaches have been demonstrated including optical-parametric-oscillators (OPO),[15–18] difference-frequency-generation (DFG),[19–25] microresonators,[26–30] quantum cascade lasers (QCLs),[31] and supercontinuum generation.[32–38] Nonetheless, there lies an opportunity for approaches demonstrating broad bandwidth mid-IR generation with the combined attributes of robust integration, low noise, high spectral resolution, and engineered spectral shape.

In the present work, we engineer supercontinuum in silicon-on-sapphire (SoS) waveguides to realize versatile and coherent mid-IR frequency combs with tunable spectral shape and coverage. This platform is introduced for mid-IR nonlinear photonics in an earlier work of Singh *et al.*[36] We build upon this initial demonstration to fully realize the strength of the SoS platform in terms of geometrical engineering of the waveguides by changing the strip waveguide dimensions and introducing a new waveguide cross section, called "notch waveguides." Through this, we achieve mid-IR frequency combs with tailored spectral shape and bandwidth. We use a series of calculations and experiments to characterize the temporal coherence and intensity noise behavior of the generated mid-IR spectra. We show that supercontinuum generation preserves the coherence of the pump frequency comb over the entire spectral band. We also demonstrate that the supercontinuum adds negligible intensity noise beyond that of the 3 μm pump, keeping relative-intensity-noise (RIN) below -90 dBc/Hz. This enables the use of our devices for dual-comb spectroscopy (DCS) of carbonyl sulfide (OCS) at 5 μm.

The motivation to use a nanophotonic platform lies in the connection between geometric control of the waveguides and the group-velocity-dispersion (GVD), which allows the unique tailoring of the nonlinear light generation with the application-defined power, spectral shape, and bandwidth. Taken together with robust lithographic fabrication, and the strong third-order-nonlinearity of Si,[36] we realize on-chip, tunable, mid-IR frequency combs across 70 THz (2.5 μm–6.2 μm) with both multi- and broad-band spectra. Furthermore, the simplicity and flexibility of the photonic technology introduced here are conducive to system-level integration with emerging chip-based DFG sources[39] or mid-IR passively mode-locked fiber sources.[40] This could lead to a heterogeneously integrated nanophotonics platform for versatile, mid-IR sources with small footprint, low power consumption, and modest cost. The user-controlled and engineered multiband spectra would particularly benefit applications where parallel multi-comb operation is desired, such as point sensors for real-time *in situ* chemical synthesis monitoring, near-field microscopy, and remote sensing.

II. WAVEGUIDE GEOMETRIES AND DISPERSION PROFILES

A silicon-based integrated photonic platform provides many characteristics required for efficient mid-IR supercontinuum generation. This includes transparency to ~8.5 μm, high third-order non-linearity ($n_2 = 6 \times 10^{-18} \frac{m^2}{W}$, which is 200× larger than silica),[36] and high index of refraction (from 3.42 to 3.45). Together, these properties lead to low intrinsic loss, high mode confinement, versatile dispersion engineering in waveguides, and enhanced nonlinear interactions. Historically, however, nonlinear Si photonics depended on Si-on-Insulator (SOI) technology in which the optical mode interacts with a SiO_2 cladding material.[37,38] This platform not only limits the geometrical dispersion by reducing the core-cladding index contrast, it also restricts the mid-IR generation to wavelengths shorter than ~4.0 μm due to the increased absorption of the oxide cladding. For this reason, alternative Si-based platforms with different cladding materials are necessary to fully realize the advantages of a Si-based nonlinear photonic platform for mid-IR applications.

We design and fabricate air-clad Si waveguides on a sapphire substrate to avoid extra losses due to cladding and substrate absorption.[36] The waveguides are tapered to wider widths for broadband input and output coupling (see Sec. I of the supplementary material for fabrication details). The propagation and coupling losses are measured at the pump wavelength to be 5 dB/cm–7 dB/cm (depending on waveguide geometry) and 6.7 dB $\pm$ 1.4 dB per facet, respectively. Two different waveguide cross sections are used for engineered dispersion profiles providing anomalous GVD at the pump wavelength of 3.06 μm. Strip waveguides with a rectangular cross section of 600 nm

height and different waveguide widths from 2.2 μm to 3.2 μm are fabricated as the first group of devices. A scanning-electron-micrograph (SEM) of a device cross section overlaid with a simulation of the input mode, and a schematic diagram of the waveguides are presented in Figs. 1(a) and 1(b), respectively. These devices have anomalous GVD profiles [Fig. 1(c)] that make them suitable for supercontinuum generation in which most of the optical power is transferred within 30 THz of the pump.

For efficient light generation above 4.2 μm (more than 30 THz away from the pump), a different approach is taken to provide an engineered zero crossing of the dispersion at long wavelengths. A second group of devices, notch waveguides, are designed and utilized for this purpose. These waveguides have a rectangular cross section with a shallow-etched notch on top [Figs. 1(d) and 1(e)]. In our designs, the waveguide width, W_{wg}, and notch depth, nD, are fixed at 3.45 μm and 300 nm, respectively. Two notch widths, W_n, of 380 nm and 530 nm are fabricated where, as shown in Fig. 1(f), the zero-dispersion wavelength is tuned with the notch position, nP, relative to the center of the waveguide.

These notch waveguides facilitate dispersive wave generation[41–44] where a significant portion of the pump energy, as high as 40% depending on the pump pulse duration,[44] is transferred into a spectral peak with its center wavelength in the normal dispersion regime. The exact wavelength of the dispersive wave depends on the pump parameters and waveguide geometry and can be tailored using the phase matching condition[45] defined by $\beta_{DW} - \beta_p - 1/v_g(\omega_{DW} - \omega_p) = 1/2\gamma P_p$. In this expression, β_{DW} and β_p are the propagation constants of the waveguide at the dispersive wave and pump wavelengths, v_g is the group velocity at pump, ω_{DW} and ω_p are the dispersive wave and pump angular frequencies, P_p is the pump peak power, γ is the waveguide nonlinearity and is given by $\gamma = \frac{n_2 \omega_p}{c A_{eff}}$ with c being the speed of light, n_2 is the nonlinear index of Si at the pump wavelength, and A_{eff} is the effective area of the waveguide.

Moreover, strip and notch waveguides can both be designed to provide flat, anomalous GVD with values close to zero in a broad wavelength bandwidth to generate octave-span continuum for applications requiring broad comb coverage. Here, in Fig. 1(g), we present two designs that facilitate this goal. The first waveguide has a strip cross section with W_{wg} = 3.06 μm (dark blue curve), while
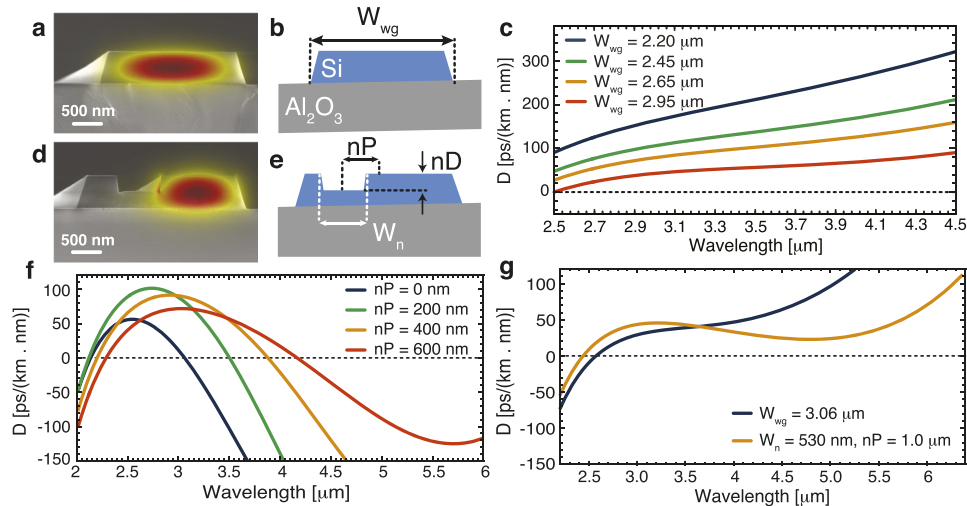

FIG. 1. Silicon-on-sapphire waveguides and calculated dispersion curves. [(a)–(c)] SEM micrograph, cross-sectional diagram, and GVD profiles of fabricated strip waveguides, respectively. These waveguides are designed for multiband light generation in targeted 3 μm–4.2 μm bands. [(d)–(f)] SEM micrograph, cross-sectional diagram, and GVD curves of fabricated notch waveguides. The long-wavelength zero dispersion point can be tuned and pushed to longer wavelengths by increasing the notch position relative to the center of the waveguide, enabling efficient light generation up to 5.7 μm. The 3 μm input modes of the waveguides are overlaid on their SEM images while the waveguide width, notch width, notch depth, and notch position are labeled with W_{wg}, W_n, nD, and nP, respectively. (g) Designed GVDs of two waveguides for octave-span supercontinuum generation. The dark blue curve is for a 3.06 μm wide strip waveguide, while the orange curve represents the GVD of a notch waveguide with W_n = 530 nm and nP = 1 μm.

the second design benefits from the notch cross section, with $W_n = 530$ nm and nP = 1 μm, to provide a flat GVD profile over a broader bandwidth (orange curve).

III. SUPERCONTINUUM GENERATION

The validity of the dispersion designs and their usefulness for broadband supercontinuum spectra is verified experimentally. We design and build a laser based on a 1550 nm erbium-fiber oscillator performing DFG in a periodically poled lithium niobate (PPLN)[19] to generate 3.06 μm pump light with 100 fs, 1 nJ pulses (refer to Sec. II of the supplementary material). The mid-IR pump beam is free-space coupled to the TE_0 mode of the waveguides, with 0.12 nJ pulse energy in the device (refer to Sec. II of the supplementary material). We monitored the output of the devices with a FTIR spectrometer to record the supercontinuum spectra. We show that the strip waveguides designed in Fig. 1(c) are optimal for light generation in multiple bands covering the spectral range from 3 μm to 4.25 μm depending on the width of the waveguide [Fig. 2(a)]. The notch waveguides are also tested, and it is shown in Fig. 2(b) that these generate long-wavelength dispersive waves, pushing the light to wavelengths as high as 5.7 μm depending on the notch position. In addition, Fig. 2(c) presents the measured output spectra of the two waveguides (strip and notch) designed for broadband, octave-span supercontinuum generation. Due to the flat GVD profile shown in Fig. 1(g), the strip waveguide provides a broad spectrum from 2.3 μm up to 5 μm, but the generated spectrum drops due to the GVD values (larger than 100 ps/km nm) at longer wavelengths. Similarly, the notch waveguide generates light at wavelengths from 2.5 μm to 6.2 μm due to its extremely flat GVD profile. Here, the combination of increasing GVD values and absorption of the sapphire substrate limit the generation at wavelengths above 6.2 μm. The output mid-IR powers of the waveguides at the shaded regions in Figs. 2(a) and 2(b) are
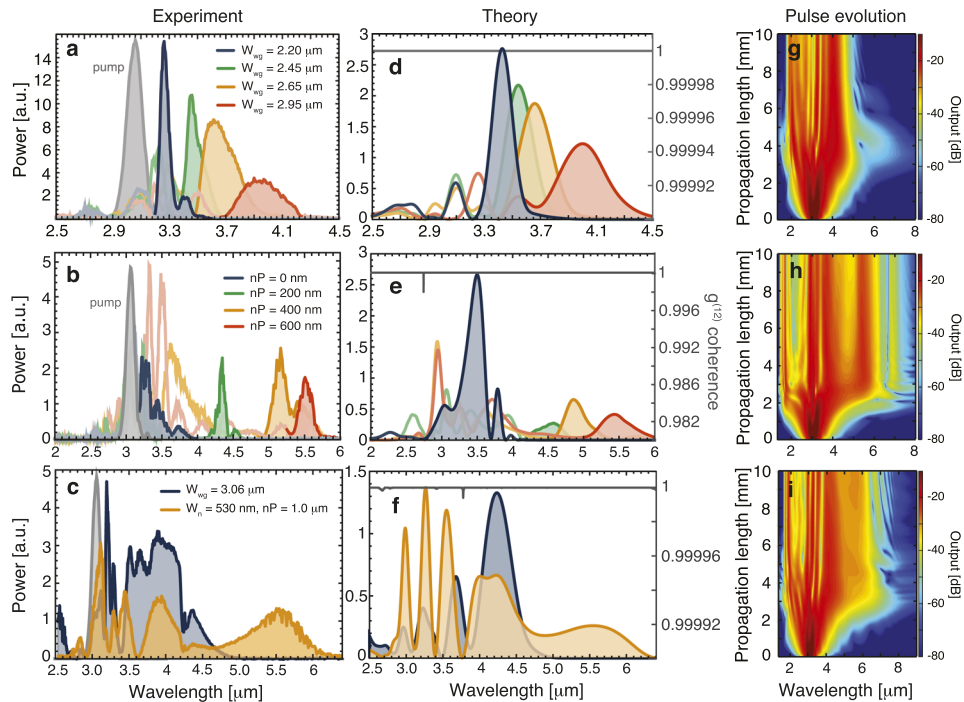

FIG. 2. Experimental and simulated supercontinuum from strip and notch SoS waveguides. [(a) and (b)] Measured output spectra of strip and notch waveguides, respectively. (c) Octave span broadening in mid-IR extending to 6.2 μm from a strip (blue curve) and notch (orange curve) waveguide. [(d)–(f)] Generalized nonlinear Schrödinger equation calculated supercontinuum spectra of the waveguide devices under investigation for strip waveguides, notch waveguides, and octave-span broadening devices, respectively. The calculated temporal coherence of the broadest spectrum in each panel is plotted with the gray line and presented on the right vertical axis. [(g)–(i)] Calculated two-dimensional frequency domain, pulse-evolution plots along the length of the waveguides. Data are presented for a strip waveguide with $W_{wg} = 2.95$ μm, notch waveguide of $W_n = 380$ nm and nP = 600 nm, and a notch waveguide of $W_n = 530$ nm and nP = 1.0 μm, respectively.

independently measured to be tens of microwatts. The spectral shape, bandwidth, and power of the shaded regions are of great importance since they can be filtered and used for dual-comb spectroscopy applications. It is worth noting that the new generation of the SoS waveguides, fabricated after preparation of this manuscript, generates 100 μW–200 μW at these spectral bands of interest due to improved coupling and propagation losses. The output spectra of the new devices can be found in Sec. III of the supplementary material. We also note that although 3 μm–5 μm mid-IR light generation is possible through DFG directly from PPLN,[23,24] the Si waveguide platform offers some distinct advantages. The Si-photonics not only enables extremely simple wavelength tunability through waveguide geometrical engineering, but it also satisfies an important spectroscopic requirement of broad bandwidth (larger than 10 THz) and flat optical spectrum (less than 10 dB spectral variation). Moreover, this platform enables having hundreds of devices with different GVD profiles on a single 1 cm^2 device area size.

We model the supercontinuum generation by solving the generalized nonlinear Schrödinger equation (gNLSE) using a split-step Fourier method.[46] The gNLSE solver includes waveguide dispersion, nonlinear phase shift, linear losses of the waveguides, three-photon-absorption (3PA), as well as 3PA-induced free carrier absorption (FCA) and dispersion (FCD) in Si[47] according to the derivation explained in Sec. IV of the supplementary material. To achieve accurate results, we implement in the calculations the measured 3.06 μm pump parameters along with the measured coupling and propagation losses of the individual devices. Figures 2(d)–2(f) show the calculated output spectra of the 1 cm long ridge waveguides, notch waveguides, and devices with octave-span broadening, respectively. The evolution of the 3.06 μm pulse propagating along different waveguides is also presented in Figs. 2(g)–2(i). The pulse evolution plots correspond to the broadest spectrum in Figs. 2(d)–2(f), respectively. We note that our supercontinuum measurements are in good agreement with the theoretical calculations, enabling us to have a precise control over the geometrical designs of the waveguides.

The pulse evolution simulations reveal that the soliton fission occurs 3 mm into the Si waveguide. While the spectral broadening in strip waveguides is mostly dominated by the soliton fission and soliton dynamics, in notch waveguides, the dispersive wave generation is responsible for the long wavelength spectral peak as predicted by the phase matching condition explained earlier. Our use of ultrashort 100 fs pulses favors the aforementioned nonlinear processes along with self-phase modulation as the main sources of supercontinuum generation. As verified theoretically and experimentally and detailed below, these processes maintain the coherence of the original pump pulse,[37] in contrast to experiments with long picosecond pulses that result in background noise amplification and pulse interaction with the generated 3PA-induced free carriers.[48] We also note that the measured and simulated spectra in Figs. 2(a)–2(f) are plotted on a linear scale to emphasize the spectral flatness of the generated mid-IR bands for DCS applications.

We calculate the coherence of our supercontinuum generated light over the entire spectral bandwidth by adding shot noise to the input pulse.[49] In such simulations, the input pulse, $E(t)$, is modified such that E(t) → E(t) + ΔE(t) with ΔE(t) being the added noise. In this method, the noise has a Gaussian-distributed random behavior in both amplitude and phase quadratures and is defined by $\Delta E(t) = E_{n0} e^{i\phi_n t}$, where E_{n0} and ϕ_n are the Gaussian-shape randomly computed intensity and phase variables, respectively. To study the coherence properties of the supercontinuum light, the first-order coherence function, $g^{(12)}(\omega)$, is calculated as[49]

$$g^{(12)}(\omega) = \frac{|\langle E_i(\omega)E_j(\omega)\rangle_{(i \neq j)}|}{\sqrt{\langle |E_i(\omega)|^2\rangle\langle |E_j(\omega)|^2\rangle}}. \tag{1}$$

We calculate this for an ensemble of 100 independently simulated spectra, although it is confirmed that the result does not change for ensembles with more than 30 spectra. This coherence function is calculated for all the waveguide outputs presented in Figs. 2(a)–2(c), but only the data corresponding to the broadest spectra of the strip, notch, and octave-span devices are presented on the right, vertical axis of Figs. 2(d)–2(f), respectively. The coherence of the original pump source is preserved across the entire optical bandwidth of all waveguide outputs within 3σ, 99.7%, of the maximum value of one.
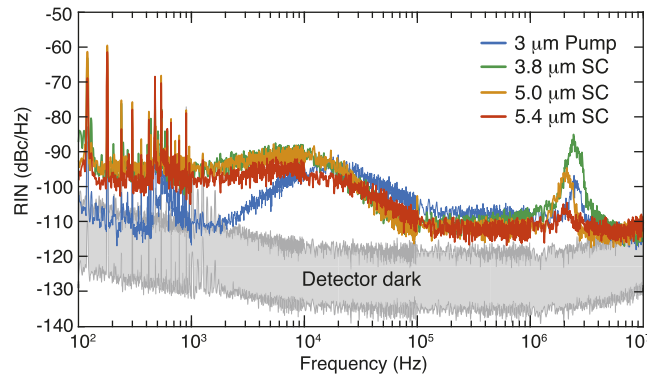
FIG. 3. The RIN data are measured for the mid-IR bands of 3.8 μm, 5.0 μm, and 5.4 μm at the output of the Si waveguides and compared with that of the 3 μm pump. The detector dark measurement is normalized to the photocurrents generated by different mid-IR bands and is presented as the shaded gray area. Dark measurements normalized to the 3.0 μm and 3.8 μm photocurrents are shown as the lower boundary of the shaded region with the 5 μm and 5.4 μm cases presented as the upper boundary. Estimated shot noise levels generally do not exceed the detector noise and lie in the range of −130 to −138 dBc/Hz, dependent on the optical powers of the mid-IR bands.

IV. INTENSITY NOISE PROPERTIES

In many spectroscopy experiments, amplitude noise present in the light source limits the achievable precision.[4] Thus, we characterize the relative-intensity-noise (RIN) for different mid-IR bands at the output of the waveguides (refer to Sec. V of the supplementary material for details of the measurement). The data are taken for a noise bandwidth of 100 Hz–10 MHz and presented in Fig. 3. The intensity noise of the waveguide outputs closely follows that of the 3.06 μm pump for frequencies above 10 kHz. At less than 10 kHz, however, there is ∼15 dB added noise at the waveguide outputs which is attributed primarily to mechanical stability and vibrations that perturb the coupling into these micron-scale waveguides. We also note a noise peak at ∼2 MHz coming from the pump source. Significantly, the measured levels of RIN stay below −90 dBc/Hz over the measurement bandwidth, which do not pose any limitation in our dual-comb spectroscopy experiments.[19]

V. DUAL COMB SPECTROSCOPY IN THE MID-IR

The low-noise nature of our waveguide-generated mid-IR light along with its spectral flatness opens numerous applications for dual-comb spectroscopy. One candidate for such a demonstration is carbonyl sulfide (OCS) with ro-vibrational lines from 4.7 μm to 5 μm.[50] We place an OCS gas cell in the beam path of a dual-comb system centered at 4.85 μm with 250 nm full-width-half-maximum (FWHM) bandwidth. The setup diagram of the dual-comb system is presented in Fig. 4(a) in which a Si waveguide generates a dispersive wave at 4.85 μm in one of the arms, called comb 1; a spectrally overlapped mid-IR light is generated directly from a PPLN crystal in the second arm, comb 2. The spectra of the Si-based and PPLN-based combs are presented in Figs. 4(b) and 4(c), respectively. The Si waveguide generates 10 μW in the presented band, while the PPLN crystal generates ∼500 μW.

The pump source of the combs originates via DFG. Therefore, the mid-IR combs are offset-free, meaning that only stabilization of the repetition rates is required to stabilize all comb lines. We lock and stabilize Δf_{rep} of the dual-comb system using a microwave circuit to enable recording and averaging of the dual-comb heterodyne signal. This was performed based on ∼10 GHz RF components operating at the 96th harmonic of the repetition rates of the two combs.[51] The details of this circuit are in the Sec. VI of the supplementary material. While this scheme has the benefit of operating with established microwave circuitry in the 10 GHz region, it is nonetheless challenging to achieve sub-half-cycle relative stability at the 600,000th harmonic of the repetition rate near 60 THz optical frequency (5 μm wavelength).
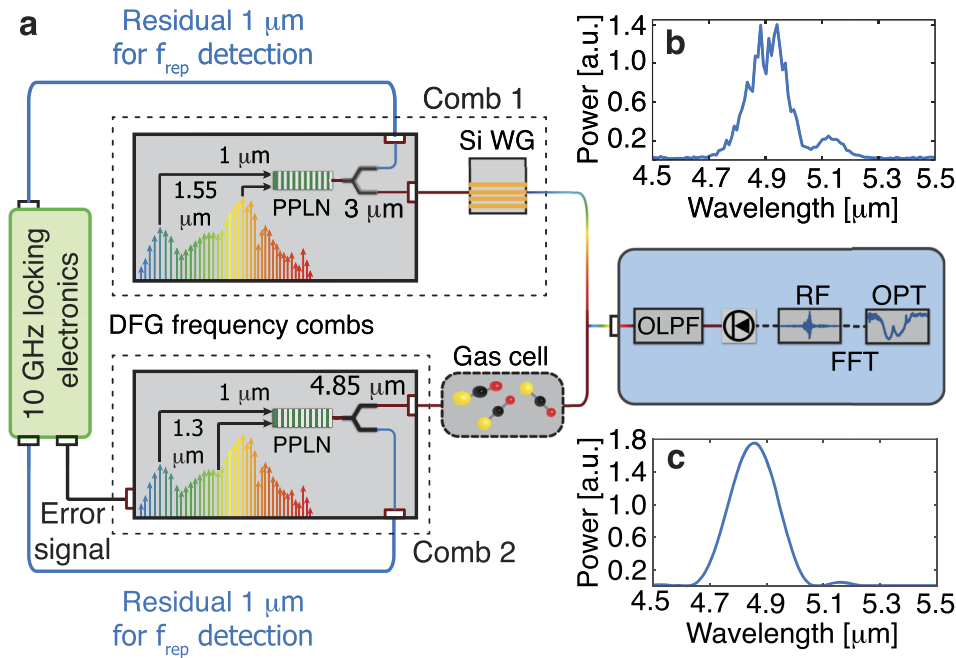
FIG. 4. Dual-comb generation and spectroscopy setup. (a) Diagram of the constructed Si-chip-based dual-comb setup. PPLN: periodically poled-lithium-niobate, WG: waveguide, OLPF: optical long-pass filter, FFT: fast-Fourier-transform, OPT: optical domain transmission. (b) Spectrum of the dispersive wave generated in the "notch" Si waveguide and used in dual-comb spectroscopy of OCS with (c) the spectrum generated from the DFG in PPLN in comb 2.

In-loop analysis of the locking noise, representing the best-case scenario for our stabilization shows a total accumulated timing jitter of 24 fs, integrated from 10 Hz to 10 MHz. This is 1.6× the optical cycle of 5 μm light or equivalently 3.2π radians of phase noise. However, most of this timing jitter is accumulated between sampling rates of 1 kHz–10 kHz. Above 10 kHz, the accumulated jitter is below 10 fs, achieving close to half-cycle relative stability. Therefore, if we choose a sampling window below 100 μs, averaging over consecutive interferogram measurements will be possible. In the experiment, we used a 20 μs acquisition window. While this is a promising result, a larger time window of $1/\Delta f_{rep}$ = 1/512 Hz = 1.95 ms is required for obtaining a comb-line resolved spectrum. Achieving a sub-half-cycle relative stabilization at 5 μm (60 THz) in this full window should be possible with improved microwave signal-to-noise and higher servo bandwidth. Additionally, improved relative stabilization along with active phase-error-correction methods such as field-programmable gate array (FPGA) units, and adaptive sampling technique,[52–54] or computational phase correction during the post-processing of the acquired data will make dual-comb spectroscopy possible at our 100 MHz comb-line-spacing resolution.

Figure 5 presents the spectroscopy results with the OCS gas sample in the beam path of the comb 2. The heterodyne beat of the dual-combs is recorded with an oscilloscope. Figure 5(a) presents 11 successive interferograms in a 20 ms time window, with each signal being separated from the neighboring beat by 1.68 ms ($1/\Delta f_{rep}$). In Fig. 5(b), Δf_{rep} is locked at 512 Hz and the acquisition window is reduced to 20 μs, of which a zoomed-in to 13 μs window is plotted for a single-shot recording with the light-blue curve. Multiple interferograms are averaged on the oscilloscope, to increase the signal-to-noise-ratio (SNR), as shown for 16,384 averages with the red curve in Fig. 5(b). The averaging is performed with triggering the scope on the center burst of the dual-comb interferogram signal. This triggering effectively aligns the center burst and removes slow jitter in Δf_{rep}. Our RF-locking scheme additionally reduces timing jitter in the 20 μs window such that we see stable interferograms with the SNR that improves with averaging.

Figure 5(c) represents the normalized optical spectrum of the dual-comb system in the presence of OCS. This is calculated from the Fourier transform of the measured interferograms with conversion of the RF frequencies to the optical domain using the values of f_{rep} and Δf_{rep}.[4] Our results are also
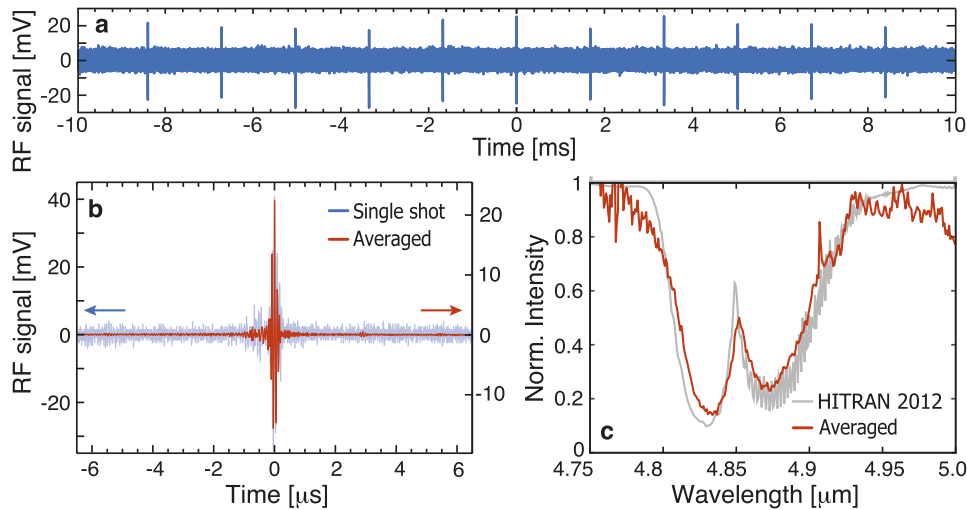
FIG. 5. Dual-comb spectroscopy results. (a) Time domain, single shot, pulse train of the dual-comb interferogram in 20 ms time span. (b) The single shot (light-blue) and 16,384 times averaged (red) center burst of the dual-comb heterodyne signal in a 13 μs time span. The single shot signal is plotted on the left vertical axis with the averaged data plotted on the right. (c) The normalized absorption spectrum of OCS is presented at 16,384-times averaging and compared with the reference spectrum from the HITRAN 2012 database. The normalized spectra in (c) are acquired by calculating the Fourier transform of the heterodyne signal in (c). The absorption spectra are normalized to that of the dual-comb system without the gas cell.

compared with that of the HITRAN 2012 database which is plotted with the gray curve. It is shown that our measurement is in good agreement with the database when the HITRAN spectrum is processed to match our 10 GHz spectral resolution (defined by the 20 μs measurement window). With improved frequency stabilization or more sophisticated phase correction,[9,52–54] our system should ultimately provide resolution at the 100 MHz comb-tooth spacing.

Finally, as noted earlier, and in the supplementary material, our newly fabricated SoS devices with 10× larger output powers will enable a comparable or greater SNR in a dual-comb setup based on two Si-waveguide generated combs. Moreover, the dual-comb signal strength is proportional to the product of the optical powers of the two mid-IR lasers. Therefore, similar SNR will be achieved if the gas sample is placed in the beam path of comb 1, generated by the Si waveguide.

VI. DISCUSSION AND OUTLOOK

We present SoS waveguides as a nonlinear photonic platform for mid-IR comb generation and spectroscopy. Through dispersion engineering, we efficiently broadcast coherent frequency comb spectra across 70 THz of bandwidth in the mid-IR with power that can be engineered on either broad or narrow spectral windows. This capability provides the means to tailor the optical spectrum for detection and analysis of specific chemical compounds or to distinguish between multiple species. The intensity noise performance and spectral flatness of the generated light enabled us to demonstrate preliminary dual-comb spectroscopy of OCS in the 5 μm spectral region. By employing suspended Si waveguides[55] or materials such as GaP and GaAs,[15,25,56] the approaches demonstrated here could be engineered and extended to provide spectral coverage beyond 10 μm.

A strength of this nanophotonics platform lies in the simple few-layer fabrication along with their versatile performance and small chip footprint of 1 cm^2, housing hundreds of devices. This platform provides many opportunities for system-level integration with a wide range of mode-locked, femtosecond-pulsed, mid-IR sources. System integration enables spectral tailoring of such sources to cover the span of the mid-IR regime from 3 μm to 10 μm in a flexible, controlled manner. For example, the emerging femtosecond-pulsed Er^{3+}-doped ZBLAN mid-IR fiber lasers[57] can be an interesting option to replace our free-space DFG-based pump. Alternatively, our nanophotonic chip can be integrated with a waveguide DFG pump to comprise a powerful nanophotonic

system for mid-IR generation and spectral tailoring.[39] Additionally, power requirements for the pump sources can be reduced through utilization of nanophotonic devices. These reductions arise from high on-chip optical intensity, better waveguide mode matching, and GVD engineering when DFG is performed on the chip. Such a chip-based coherent infrared light source will expand applications in a range of laboratory spectroscopy, lab-on-a-chip diagnostics, and scanning probe microscopy.

SUPPLEMENTARY MATERIAL

See supplementary material for a detailed description of SoS waveguide fabrication, optical measurement setup and pump source used in supercontinuum generation, theoretical analysis of the mid-IR generated spectra, and details of the RF locking scheme used in the dual-comb experiment. The results of the new generation SoS waveguides with improved output powers can also be found in Sec. III of the supplementary material.

ACKNOWLEDGMENTS

[1] T. W. Hänsch, Rev. Mod. Phys. **78**, 1297 (2006).

[2] J. L. Hall, Rev. Mod. Phys. **78**, 1279 (2006).

[3] S. T. Cundiff and J. Ye, Rev. Mod. Phys. **75**, 325 (2003).

[4] I. Coddington, N. Newbury, and W. Swann, Optica **3**, 414 (2016).

[5] F. Keilmann, C. Gohle, and R. Holzwarth, Opt. Lett. **29**, 1542 (2004).

[6] T. Ideguchi, Opt. Photonics News **28**, 32 (2016).

[7] M. J. Thorpe, K. D. Moll, R. J. Jones, B. Safdi, and J. Ye, Science **311**, 1595 (2006).

[8] S. A. Diddams, L. Hollberg, and V. Mbele, Nature **445**, 627 (2007).

[9] J. Roy, J.-D. Deschênes, S. Potvin, and J. Genest, Opt. Express **20**, 21932 (2012).

[10] P. Giaccari, J.-D. Deschênes, P. Saucier, J. Genest, and P. Tremblay, Opt. Express **16**, 4347 (2008).

[11] S. Okubo, K. Iwakuni, H. Inaba, K. Hosaka, A. Onae, H. Sasada, and F.-L. Hong, Appl. Phys. Express **8**, 082402 (2015).

[12] B. J. Bjork, T. Q. Bui, O. H. Heckl, P. B. Changala, B. Spaun, P. Heu, D. Follman, C. Deutsch, G. D. Cole, M. Aspelmeyer, M. Okumura, and J. Ye, Science **354**, 444 (2016).

[13] B. Bernhardt, A. Ozawa, P. Jacquet, M. Jacquey, Y. Kobayashi, T. Udem, R. Holzwarth, G. Guelachvili, T. W. Hansch, and N. Picque, Nat. Photonics **4**, 55 (2010).

[14] A. Schliesser, N. Picque, and T. W. Hansch, Nat. Photonics **6**, 440 (2012).

[15] L. Maidment, P. G. Schunemann, and D. T. Reid, Opt. Lett. **41**, 4261 (2016).

[16] N. Leindecker, A. Marandi, R. L. Byer, K. L. Vodopyanov, J. Jiang, I. Hartl, M. Fermann, and P. G. Schunemann, Opt. Express **20**, 7046 (2012).

[17] F. Adler, K. C. Cossel, M. J. Thorpe, I. Hartl, M. E. Fermann, and J. Ye, Opt. Lett. **34**, 1330 (2009).

[18] K. L. Vodopyanov, E. Sorokin, I. T. Sorokina, and P. G. Schunemann, Opt. Lett. **36**, 2275 (2011).

[19] F. C. Cruz, D. L. Maser, T. Johnson, G. Ycas, A. Klose, F. R. Giorgetta, I. Coddington, and S. A. Diddams, Opt. Express **23**, 26814 (2015).

[20] A. Sell, R. Scheu, A. Leitenstorfer, and R. Huber, Appl. Phys. Lett. **93**, 251107 (2008).

[21] M. A. Gubin, A. N. Kireev, A. V. Konyashchenko, P. G. Kryukov, A. S. Shelkovnikov, A. V. Tausenev, and D. A. Tyurikov, Appl. Phys. B **95**, 661 (2009).

[22] P. Maddaloni, P. Malara, G. Gagliardi, and P. D. Natale, New J. Phys. **8**, 262 (2006).

[23] S. M. Foreman, D. J. Jones, and J. Ye, Opt. Lett. **28**, 370 (2003).

[24] C. Erny, K. Moutzouris, J. Biegert, D. Kühlke, F. Adler, A. Leitenstorfer, and U. Keller, Opt. Lett. **32**, 1138 (2007).

[25] G. Insero, C. Clivati, D. D'Ambrosio, P. D. Natale, G. Santambrogio, P. G. Schunemann, J.-J. Zondy, and S. Borri, Opt. Lett. **41**, 5114 (2016).

[26] A. G. Griffith, R. K. Lau, J. Cardenas, Y. Okawachi, A. Mohanty, R. Fain, Y. H. D. Lee, M. Yu, C. T. Phare, C. B. Poitras, A. L. Gaeta, and M. Lipson, Nat. Commun. **6**, 6299 (2015).

[27] C. Y. Wang, T. Herr, P. Del'Haye, A. Schliesser, J. Hofer, R. Holzwarth, T. W. Hänsch, N. Picqué, and T. Kippenberg, Nat. Commun. **4**, 1345 (2013).

[28] K. Luke, Y. Okawachi, M. R. E. Lamont, A. L. Gaeta, and M. Lipson, Opt. Lett. **40**, 4823 (2015).

[29] M. Yu, Y. Okawachi, A. G. Griffith, M. Lipson, and A. L. Gaeta, Optica **3**, 854 (2016).

[30] M. Yu, Y. Okawachi, A. G. Griffith, N. Picqué, M. Lipson, and A. L. Gaeta, e-print arXiv:1610.01121 (2016).

[31] A. Hugi, G. Villares, S. Blaser, H. C. Liu, and J. Faist, Nature **492**, 229 (2012).
[32] C. R. Petersen, U. Møller, I. Kubat, B. Zhou, S. Dupont, J. Ramsay, T. Benson, S. Sujecki, N. Abdel-Moneim, Z. Tang, D. Furniss, A. Seddon, and O. Bang, Nat. Photonics **8**, 830 (2014).
[33] Y. Yu, X. Gai, T. Wang, P. Ma, R. Wang, Z. Yang, D.-Y. Choi, S. Madden, and B. Luther-Davies, Opt. Mater. Express **3**, 1075 (2013).
[34] T. Cheng, K. Nagasaka, T. H. Tuan, X. Xue, M. Matsumoto, H. Tezuka, T. Suzuki, and Y. Ohishi, Opt. Lett. **41**, 2117 (2016).
[35] D. D. Hickstein, H. Jung, D. R. Carlson, A. Lind, I. Coddington, K. Srinivasan, G. G. Ycas, D. C. Cole, A. Kowligy, C. Fredrick, S. Droste, E. S. Lamb, N. R. Newbury, H. X. Tang, S. A. Diddams, and S. B. Papp, Phys. Rev. Appl. **8**, 014025 (2017).
[36] N. Singh, D. D. Hudson, Y. Yu, C. Grillet, S. D. Jackson, A. Casas-Bedoya, A. Read, P. Atanackovic, S. G. Duvall, S. Palomba, B. Luther-Davies, S. Madden, D. J. Moss, and B. J. Eggleton, Optica **2**, 797 (2015).
[37] B. Kuyken, T. Ideguchi, S. Holzner, M. Yan, T. W. Hansch, J. Van Campenhout, P. Verheyen, S. Coen, F. Leo, R. Baets, G. Roelkens, and N. Picque, Nat. Commun. **6**, 6310 (2015).
[38] R. K. W. Lau, M. R. E. Lamont, A. G. Griffith, Y. Okawachi, M. Lipson, and A. L. Gaeta, Opt. Lett. **39**, 4518 (2014).
[39] A. S. Mayer, C. R. Phillips, C. Langrock, A. Klenner, A. R. Johnson, K. Luke, Y. Okawachi, M. Lipson, A. L. Gaeta, M. M. Fejer, and U. Keller, Phys. Rev. Appl. **6**, 054009 (2016).
[40] X. Zhu, G. Zhu, C. Wei, L. V. Kotov, J. Wang, M. Tong, R. A. Norwood, and N. Peyghambarian, J. Opt. Soc. Am. B **34**, A15 (2017).
[41] J. M. Dudley, G. Genty, and S. Coen, Rev. Mod. Phys. **78**, 1135 (2006).
[42] M. Bache, O. Bang, B. B. Zhou, J. Moses, and F. W. Wise, Phys. Rev. A **82**, 063806 (2010).
[43] G. Chang, L.-J. Chen, and F. X. Kärtner, Opt. Express **19**, 6635 (2011).
[44] G. Chang, L.-J. Chen, and F. X. Kärtner, Opt. Lett. **35**, 2361 (2010).
[45] D. Yoon Oh, K. Y. Yang, C. Fredrick, G. Ycas, S. A. Diddams, and K. J. Vahala, Nat. Commun. **8**, 13922 (2017).
[46] Q. Lin, O. J. Painter, and G. P. Agrawal, Opt. Express **15**, 16604 (2007).
[47] S. Pearl, N. Rotenberg, and H. M. van Driel, Appl. Phys. Lett. **93**, 131102 (2008).
[48] B. Kuyken, X. Liu, R. M. Osgood, R. Baets, G. Roelkens, and W. M. J. Green, Opt. Express **19**, 20172 (2011).
[49] A. Ruehl, M. J. Martin, K. C. Cossel, L. Chen, H. McKay, B. Thomas, C. Benko, L. Dong, J. M. Dudley, M. E. Fermann, I. Hartl, and J. Ye, Phys. Rev. A **84**, 011806 (2011).
[50] L. Rothman, I. Gordon, Y. Babikov, A. Barbe, D. C. Benner, P. Bernath, M. Birk, L. Bizzocchi, V. Boudon, L. Brown, A. Campargue, K. Chance, E. Cohen, L. Coudert, V. Devi, B. Drouin, A. Fayt, J.-M. Flaud, R. Gamache, J. Harrison, J.-M. Hartmann, C. Hill, J. Hodges, D. Jacquemart, A. Jolly, J. Lamouroux, R. L. Roy, G. Li, D. Long, O. Lyulin, C. Mackie, S. Massie, S. Mikhailenko, H. Müller, O. Naumenko, A. Nikitin, J. Orphal, V. Perevalov, A. Perrin, E. Polovtseva, C. Richard, M. Smith, E. Starikova, K. Sung, S. Tashkun, J. Tennyson, G. Toon, V. Tyuterev, and G. Wagner, J. Quant. Spectrosc. Radiat. Transfer **130**, 4 (2013).
[51] R. Gebs, G. Klatt, C. Janke, T. Dekorsy, and A. Bartels, Opt. Express **18**, 5974 (2010).
[52] T. Ideguchi, A. Poisson, G. Guelachvili, N. Picqué, and T. W. Hänsch, Nat. Commun. **5**, 3375 (2014).
[53] T. Yasui, R. Ichikawa, Y.-D. Hsieh, K. Hayashi, H. Cahyadi, F. Hindle, Y. Sakaguchi, T. Iwata, Y. Mizutani, H. Yamamoto, K. Minoshima, and H. Inaba, Sci. Rep. **5**, 10786 (2015).
[54] T. Ideguchi, A. Poisson, G. Guelachvili, T. W. Hänsch, and N. Picqué, Opt. Lett. **37**, 4847 (2012).
[55] J. Chiles, S. Khan, J. Ma, and S. Fathpour, Appl. Phys. Lett. **103**, 151106 (2013).
[56] W. C. Hurlbut, Y.-S. Lee, K. L. Vodopyanov, P. S. Kuo, and M. M. Fejer, Opt. Lett. **32**, 668 (2007).
[57] S. Duval, M. Bernier, V. Fortin, J. Genest, M. Piché, and R. Vallée, Optica **2**, 623 (2015).